TTF based donor-pi-acceptor dyads synthesized for NLO applications

Awatef Ayadi, Adam Szukalski, Abdelkrim El-Ghayoury, Karolina Haupa, Nabil Zouari, Jaroslaw Mysliwiec, François Kajzar, Bohdan Kulyk, Bouchta Sahraoui

TTF based donor-pi-acceptor dyads synthesized for NLO Applications

Awatef Ayadi[a,b], Adam Szukalski[c], Abdelkrim El-Ghayoury[a*], Karolina Haupa[d], Nabil Zouari[b], Jaroslaw Myśliwiec[c], Francois Kajzar[a], Bohdan Kulyk[a] and Bouchta Sahraoui[a*]

[a] *Laboratoire MOLTECH-Anjou, Université d'Angers, UFR Sciences, UMR 6200, CNRS, Bât. K, 2 Bd. Lavoisier, 49045 Angers Cedex, France.*

[b] *Laboratoire de Physico-chimie de l'état solide, Université de Sfax, Route de Soukra; Km 4; BP: 802, 3038, Sfax, Tunisia.*

[c] *Faculty of Chemistry, Department of Engineering and Advanced Materials Modelling, Wroclaw University of Technology, Wyb. Wyspianskiego 27, 50-320 Wroclaw, Poland.*

[d] *Department of Applied Chemistry and Institute of Molecular Science, National Chiao Tung University, 1001, Ta-Hsueh Road, Hsinchu 30010, Taiwan.*

Corresponding author: Abdelkrim El-Ghayoury e-mail : abdelkrim.elghayoury@univ-angers.fr
Bouchta Sahraoui e-mail : bouchta.sahraoui@univ-angers.fr

Abstract

Two new TTF-pi-acceptor dyads that contain *p*-nitrophenyl group as acceptor and bis-(styryl)benzene system as an efficient π–conjugated bridge have been synthesized by multistep synthetic procedure and their electrochemical behavior has been studied by cyclic voltammetry (CV). The occurrence of an intramolecular charge transfer (ICT) in these molecules has been evidenced by UV-Visible electronic absorption spectroscopy and these studies were completed by DFT calculations in both gas phase and in solution. The nonlinear optical parameters obtained via SHG and THG measurements are described and indicate that these materials are valuable candidates for the construction of optoelectronic and photonic devices. The Optical Kerr Effect measurements indicate that these materials exhibit a great potential in the field of optical switchers construction, where the material's photoresponse time is a crucial parameter.

1. Introduction

Push-Pull organic molecules which contain an electron donor (D) and an electron acceptor (A) units that are covalently linked by a π-conjugated bridging group (D-π-A systems) exhibiting intramolecular charge transfer (ICT) states have attracted considerable attention because of their possible use as organic optical and electronic functional materials with low energy-gap[1]. Tetrathiafulvalene (TTF) derivatives, which are known to exhibit, in addition to the neutral state, two one-electron reversible oxidation states (i.e. the stable radical cation $TTF^{+\bullet}$ and dication TTF^{2+}) are very useful and versatile π electron donating units and play therefore a major role in the preparation of molecular materials designed for various applications. They have been, for example, used as electron donor molecules to prepare (super)conducting crystalline materials[2-5], as redox switches in molecular and supramolecular architectures [6-10], as donor components for photovoltaic devices [11-12] as well as donor moieties in nonlinear optical (NLO) materials [13-16]. For these later materials, numerous studies have shown the important role of both the electron donor and the electron acceptor moieties. Lately, the modulation of the electrooptic coefficient with temperature and pressure has been observed in TTF-derivatized fullerenes [17]. Very recently we have been interested in the use of TTF based ligands, which can also be considered as donor-π-acceptor systems, in order to tune their electronic properties as well as their nonlinear optical response upon metal complexation. We have therefore shown an increase of the nonlinear optical behavior of orthogonal tetrathiafulvalene (TTF)-based ligands by the complexation with platinum as compared with palladium [18]. In the case of TTF-based iron and ruthenium metal complexes we have observed a switching of the nonlinear absorption character of the systems from Saturable Absorptive to Reverse Saturable Absorptive behavior upon metal complexation [19]. Moreover, we have recently shown an increase of the nonlinear optical response of TTF-based bis-iminopyridine ligand coordinated with zinc(II) metal cation [20]. It is well established that in the field of donor-π-acceptor molecular structures different design principles are proposed to enhance the nonlinear absorption within a variety of conjugated molecular structures. For this purpose we have selected the TTF moiety as donor part because of the aforementioned properties of these derivatives and nitrophenyl accepting group which has been utilized in many efficient donor-acceptor materials. Also of great importance is the choice of the π-conjugated spacer which plays a crucial role for the efficient

electronic communication between the donor and the acceptor parts [21]. It has been shown that the bis-(styryl)benzene (BSB) system acts as an efficient conjugated π–bridge for NLO materials in which donor (D) and/or acceptor (A) substituents are connected in a symmetrical (D-π-D, A-π-A) or asymmetrical (D-π-A) arrangements. As the continuation of our research on the preparation of suitable materials for nonlinear optical applications, we report herein on the synthesis, characterization, theoretical calculations and experimental study of nonlinear optical properties of two TTF-based donor-pi-acceptor systems (Scheme 1) which demonstrate high nonlinear optical response.

DA-1 (R = H); DA-2 (R=CH₃).
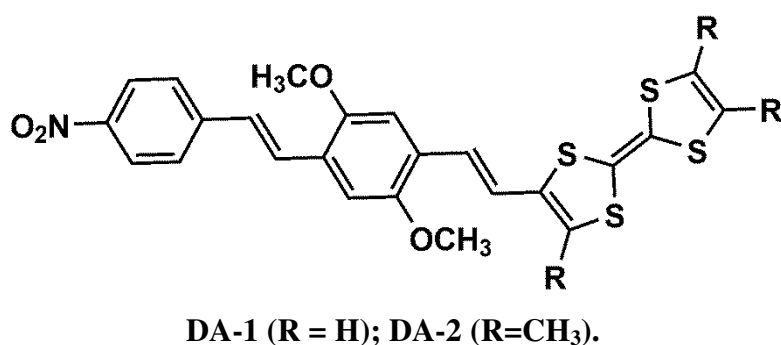
Scheme 1. Chemical structure of the two D-π-A compounds.

2. Experimental

2.1. Chemicals and characterization techniques

Commercially available reagents and all solvents for synthesis were of analytical grade and were used without further purification. Reactions were carried out under nitrogen. Nuclear magnetic resonance spectra were recorded on a Bruker 300 MHz spectrometer. The following abbreviations are used to represent the multiplicity of the signals: s (singlet), d (doublet), the spin-spin coupling constants (J) were measured. Infrared spectra were recorded on a Bruker vertex 70 spectrometer, the measurements were recorded in 400 to 4000 cm^{-1} range. Elemental analyses (C, H and N) were performed on a Thermo-Scientific Flash 2000 Organic. Mass spectrometry measurements were performed on a Bruker Biflex-III TM which uses 1,8,9-trihydroxyanthracene as matrix. UV-Visible absorption spectra were recorded at room temperature in quartz cuvettes using Perkin Elmer spectrophotometer. Cyclic voltammetry (CV) experiments were performed in a three-electrode cell equipped with a platinum millielectrode as the working electrode, a platinum wire as a counter electrode and a silver wire Ag/Ag+ used as a reference electrode. The electrolytic media involved a 0.1 mol/L solution of (n-Bu₄N)PF₆ in dichloromethane. Melting points were measured with a Melting Point Apparatus SMP3.

2.2. Computational details

The geometry of *cis and trans* isomers of investigated molecules was performed using the Gaussian09 software [22]. The B3LYP functional with 6-311(d,p) basis set was used for the gas phase calculations. The calculations in DCM (dichloromethane) solution were done using the PCM model (*Polarizable Continuum Model*) [23] as implemented in the Gaussian09 package [24]. The nature of the optimized geometries at the B3LYP level was checked by vibrational frequency calculations. The vibrational frequencies were calculated for all minima on PES (Potencial Energy Surface) which were confirmed to have zero imaginary frequency. Obtained relative energies include zero point vibrational energy (ZPVE) corrections. The abundances of the found conformers at the room temperature were calculated according to the Boltzmann distribution. The polarizabilities and hyperpolarizabilities were computed using static frequencies. Simulated UV-Vis absorption spectra were obtained by TD-DFT (B3LYP and CAM-B3LYP) method using optimized geometry.

2.3. NLO experiments

As the first step of NLO investigations the frequency doubling generation experiments have been conducted. Typical experimental set-up for such purpose has been used as previously described [25]. In our case the fundamental beam of picosecond Nd:YVO$_4$ laser (λ = 1064 nm) was irradiating the samples, which were positioned on the rotational stage. The incident beam was controlled by the set of polarizers, half-wave plates, lenses and electronic system, which synchronized incidental and generated beam. From the reason of structural demands for the 2nd order nonlinear optical effects additional particular procedure was done to prepare samples for this experiment. It was necessary to align molecules in defined direction in order to break centrosymmetry inside volume of the polymeric film. To achieve this alignment of *push-pull* type molecules we have used corona poling technique (T = 83° C, heating time: 15 minutes).

3. Results and discussion

3.1. Synthesis

The synthesis of the starting precursor (a) was carried out according to the previously described procedures [26]. The synthesis of **b**, **c** and **d** (Scheme 2) was inspired from the work published by Fabbrini *et al.* [21]. TTF aldehydes **e** [27] and **f** [28] were prepared according to literature procedures. Thus, the 4-(hydroxymethyl)-2,5-dimethoxybenzaldehyde (a) was reacted with diethyl-4-nitrobenzylphosphonate in the presence of *t*-BuOK in dry dimethylfomramide (DMF), under Horner-Wadsworth-Emmons conditions to give the intermediate **b**. Subsequent bromination with phosphorus tribromide in tetrahydrofurane solution gave (E)-1-(bromomethyl)-2,5-dimethoxy-4-(4-nitrostyryl)benzene **c** in 70% yield. The reaction of triphenylphosphine with **c** afforded (E)-(2,5-dimethoxy-4-(4nitrostyryl)benzyl) triphenylphosphonium bromide **d** which was used in a Wittig reaction with TTF aldehydes (**e** and **f**) to afford **DA-1** and **DA-2** in 57% and 65% respectively.
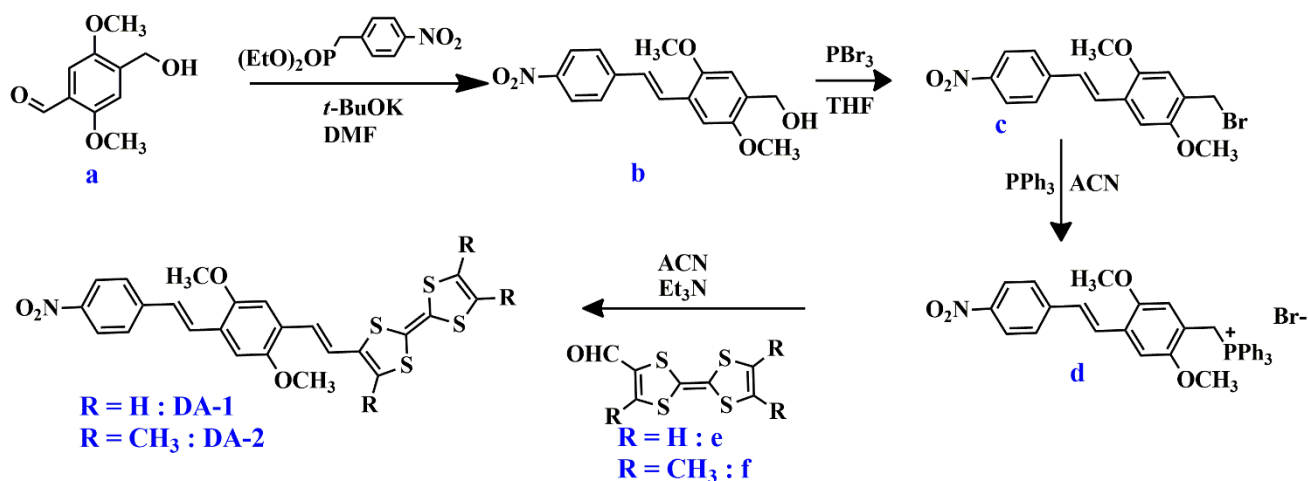
Scheme 2: Synthetic route of compounds **DA-1** and **DA-2**.

Synthesis of (E)-(2,5-dimethoxy-4-(4-nitrostyryl)phenyl)methanol: b

In a three-necked flask under nitrogen, diethyl-4-nitrobenzylphosphonate (348 mg, 1.274 mmol) was suspended in dry DMF (10 ml), a solution of t-BuOK (355 mg, 3.17 mmol) was added dropwise. The mixture was stirred for few minutes then, a solution of 4-(hydroxymethyl)-2,5-dimethoxybenzaldehyde (250 mg, 1.274 mmol) was added. The mixture was stirred overnight and 50 ml of water was then added, the resulting mixture was stirred for additional 10 minutes. The orange solid was filtered and purified by column chromatography (petroleum ether/ ethyl acetate 7/3) to give compound **b** as an orange powder in 49%. Mp 130 °C; ^{1}H NMR (300 MHz, CDCl$_3$) δ = 8.25 (d, 2H, J= 8.79Hz), 7.70 (s, 1H), 7.66 (d, 2H, J= 6.83 Hz), 7.15 (m, 2H), 6.98 (s, 1H), 4.75 (s, 2H), 3.94 (s, 3H), 3.93 (s, 3H), 3.80 (s, 1H). Selected IR bands (cm^{-1}): 3279, 2833, 1628, 1588, 1507, 1462, 1411,

1337, 1318, 1285, 1209, 1176, 1109, 1041, 968, 955, 870, 829, 749, 681, 669, 502. Anal. calcd for $C_{17}H_{17}NO_5$: C, 64.75; H, 5.43; N, 4.44, found: C, 63.83; H, 5.72; N, 4.04. MALDI-TOF MS calcd: m/z = 315.32 Da. found: m/z 315.

*Synthesis of (E)-1-(bromomethyl)-2,5-dimethoxy-4-(4-nitrostyryl)benzene: **c***

In a three-necked flask under nitrogen, a solution of (E)-(2,5-dimethoxy-4-(4-nitrostyryl)phenyl)methanol (120 mg, 0.380 mmol) in (10 ml) of THF was cooled to 0°C. Then, a solution of PBr$_3$ (122 mg, 0.452 mmol) was added dropwise. The mixture was stirred for a further 10 min and 2 hours at room temperature. The solvent was evaporated under vacuum to afford an orange solid. The crude product was purified by column chromatography (petroleum ether/ ethyl acetate 6/4) to afford **c** as dark orange powder in 69%. Mp 152 °C; ^{1}H NMR (300 MHz, CDCl$_3$) δ = 8.24 (d, 2H, J= 8.83Hz), 7.68 (d, 2H, J= 8.88 Hz), 7.61 (s, 1H), 7.21 (s, 1H), 6.95 (s, 1H), 4.61 (s, 2H), 3.97 (s, 3H), 3.92 (s, 3H). Selected IR bands (cm^{-1}): 3045, 2943, 2833, 1724, 1623, 1586, 1511, 1463, 1411, 1332, 1318, 1261, 1213, 1179, 1105, 1041, 975, 955, 866, 848, 829, 748, 697, 686, 659, 555, 501. Anal. calcd for $C_{17}H_{16}NO_4Br$: C, 53.99; H, 4.26; N, 3.70, found: C, 53.63; H, 3.94; N, 3.39. MALDI-TOF MS calcd: m/z = 378.2 Da. found: m/z = 378.0 [M]$^+$.

*Synthesis of (E)-(2,5-dimethoxy-4-(4-nitrostyl)benzyl)triphenylphosphonium bromide: **d***

In a three-necked flask under nitrogen, (E)-1-(bromomethyl)-2,5-dimethoxy-4-(4-nitrostyryl)benzene (250 mg, 0.66 mmol) was suspended in dry ACN (20 ml), a solution of PPh$_3$ (363 mg, 1.65 mmol) was added dropwise. The mixture was refluxed overnight. After cooling to room temperature, the crude product was filtrated and washed with diethyl ether to yield **d** as yellow powder in 90% yield. Mp 245 °C; ^{1}H NMR (300 MHz, DMSO-d$_6$) δ = 8.23 (d, 2H, J= 8.79Hz), 7.53 (d, 2H, J= 5.29 Hz), 7.74 (m, 16H), 7.41 (m, 1H), 7.25 (s, 1H), 6.72 (d, 1H, J= 2.41Hz), 4.99 (d, 2H, J= 15.26), 3.49 (s, 3H), 3.35 (s, 3H). ^{13}C NMR (75 MHz, DMSO-d$_6$) δ =151.3, 151.2, 150.6, 150.5, 146.2, 144, 134.9, 134, 133.9, 133.3, 133.1, 130, 129.8, 128.9, 128.8, 128.7, 127.8, 127.2, 126.8, 126.7, 125.6, 124.1, 118.7, 117.5, 117, 116.8, 115.8, 115.8, 109.2, 109.1, 55.8, 55.1. Selected IR bands (cm^{-1}): 3372, 2837, 2773, 2933, 1734, 1587, 1590, 1512, 1468, 1437, 1409, 1294, 1222, 1188, 1106, 1041, 991, 871, 850, 747, 716, 685, 648, 570, 520, 504, 493. Anal. calcd for $C_{35}H_{31}NO_4BrP$: C, 65.63; H, 4.88; N, 2.19, found: C, 64.73; H, 4.84; N, 1.73. MALDI-TOF MS for $C_{35}H_{31}NO_4P$: calcd: m/z = 560.19 Da. found: m/z = 560.4 [M]$^+$.

*Synthesis of 4-((E)-2,5-dimethoxy-4-((E)-4-nitrostyryl)styryl)-2,2'-bi(1,3-dithiolylidene): **DA-1***

To a solution of (E)-(2,5-dimethoxy-4-(4-nitrostyryl)benzyl)triphenylphosphonium bromide (200 mg, 0.321 mmol) in dry acetonitrile, under nitrogen, a few drops of triethylamine was added. The resulting solution was stirred for 30 min then a solution of [2,2'-bi(1,3-dithiolylidene)]-4-carbaldehyde **e** (60.4 mg, 0.260 mmol) in dry acetonitrile was added. The mixture was then refluxed overnight. After cooling to room temperature the desired product was separated by filtration. **DA-1** was obtained as a dark powder in 57% yield, (76.18 mg, 0.148 mmol). Mp 242 °C; ^{1}H NMR (300 MHz, CDCl$_3$) δ = 8.24 (d, 2H, J = 8.7 Hz), 7.69 (d, 2H, J = 8.57 Hz), 7.36 (s, 1H), 7.23 (s, 1H), 7.13 (m, 2H), 7.01 (d, 1H, J = 5.1 Hz), 6.71 (d, 1H, J = 15.7 Hz), 6.43 (s, 1H), 6.37 (s, 2H), 3.96 (s, 3H), 3.95 (s, 3H). ^{13}C NMR (75 MHz, CDCl$_3$) δ =151.8, 151.6, 127.8, 126.9, 126.8, 126.7, 124.1, 121.7, 120.3, 119.1, 118.7, 109.5, 109.4, 109.3, 56.2. Selected IR bands (cm^{-1}): 2828, 1619, 1581, 1505, 1330, 1202, 1043, 642, 502. Anal. calcd for C$_{24}$H$_{19}$NO$_4$S$_4$: C, 56.12; H, 3.73; N, 2.73, found: C, 55.40; H, 3.65; N, 2.85. MALDI-TOF MS calcd: m/z = 513.01 Da. found: m/z = 513.3 [M]$^+$. HR-MS (M): for C$_{24}$H$_{19}$NO$_4$S$_4$: = 513.0197. Found 513.0191.

Synthesis of 4-((E)-2,5-dimethoxy-4-((E)-4-nitrostyryl)styryl)-4',5,5'-trimethyl-2,2'-bi(1,3-dithiolylidene): **DA-2**

This compound was prepared by following the same procedure as for compound **DA-1**, using 4',5,5'-trimethyl-[2,2'-bi(1,3-dithiolylidene)]-4-carbaldehyde **f**. Yield (65%); mp 265 °C; ^{1}H NMR (300 MHz, DMSO-d$_6$) δ = 8.25 (d, 2H, J=8.66 Hz), 7.85 (d, 2H, J= 8.94 Hz), 7.59 (q, 2H, J = 16.9 Hz), 7.39 (s, 2H), 7.33 (d, 1H, J= 16 Hz), 6.59 (d, 1H, J= 15.7 Hz), 3.93 (s, 3H), 3.92 (s, 3H), 2.29 (s, 3H), 1.98 (s, 6H). Selected IR bands (cm^{-1}): 2909, 1624, 1585, 1503, 1332, 1213, 1038, 632, 503. Anal. calcd for C$_{27}$H$_{25}$NO$_4$S$_4$: C, 58.35; H, 4.53; N, 2.52, found: C, 58.04; H, 4.53; N, 2.52. MALDI-TOF MS calcd: m/z = 555.06 Da. found: m/z = 555.4 [M]$^+$. HR-MS (M): for C$_{35}$H$_{31}$NO$_4$BrP: = 555.0666. Found 555.0654.

3.2. UV-Visible absorption spectroscopy

The UV–Visible absorption spectra of compounds **DA-1** and **DA-2** were recorded in dichloromethane solution with C = 4 × 10^{-5} M and C = 4.5 × 10^{-5} M, respectively, at room temperature (Figure 1). Both compounds exhibit tow strong electronic absorption bands at 331 and 422 nm for **DA-1** and 337 and 420 nm for **DA-2**, which are assigned to the π→π* and n→π* transitions resulting from the different units of the two compounds (TTF moiety, phenyl ring and the dimethoxybenzene group). This behavior is similar to that observed for the corresponding nitro-substituted *p*-phenylene vinylene oligomer [29]. In addition a shoulder is observed for both

compounds around 500 nm which might be assigned to an intramolecular charge transfer (ICT) between the TTF moiety and the *p*-nitrophenyl unit.
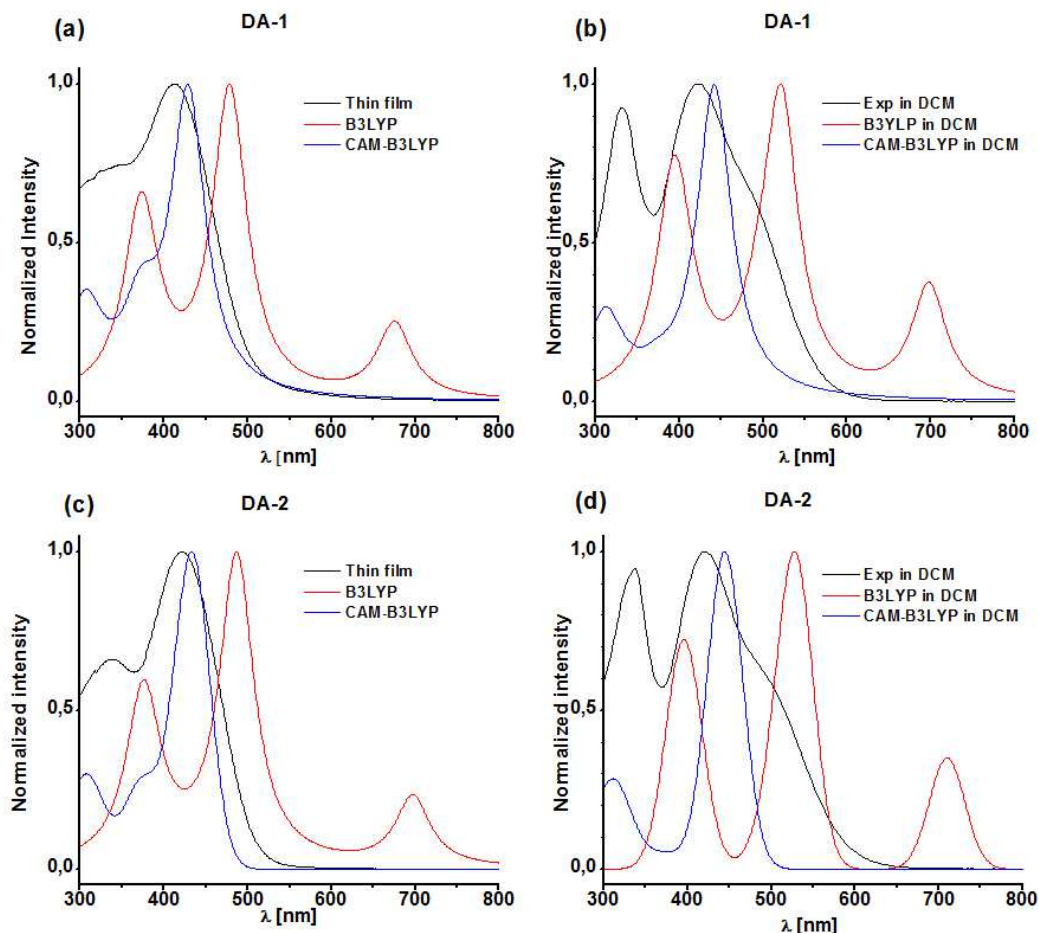
Figure 1. Experimental and theoretical absorption spectra of **DA-1** thin film (a), **DA-1** in DCM solution (b), **DA-2** thin film (c) and **DA-2** in DCM solution (d) at B3LYP and CAM-B3LYP/6-311(d,p) level of theory.

3.3. Cyclic voltametry

The electrochemical behavior of the two compounds **DA-1** and **DA-2** was examined by cyclic voltammetry (CV) (Figure 2). This measurement shows the usual two reversible one-electron oxidations of the TTF unit, which correspond to the successive formation of a radical cation at 0.35 and 0.28 V vs Ag/Ag$^+$ and a dication at 0.84 and 0.75 V vs Ag/Ag$^+$ for **DA-1** and **DA-2**, respectively. Note that E_{ox1} of **DA-1** is anodically shifted when compared with E_{ox1} of **DA-2** because of the positive inductive effect of the trimethyl groups in **DA-2**.
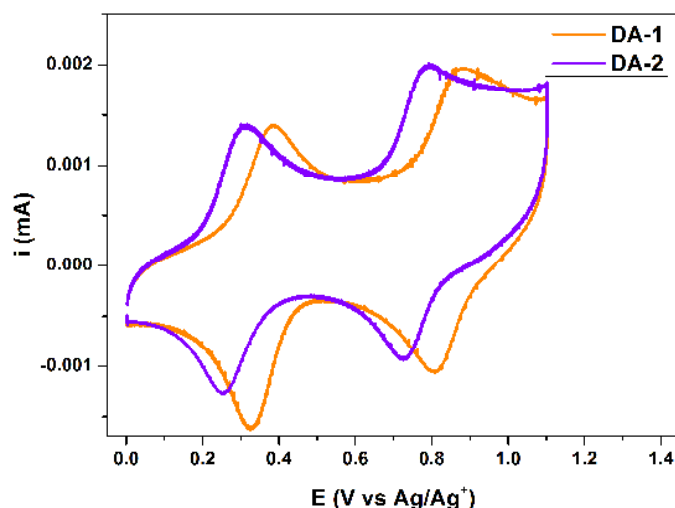
Figure 2: Cyclic voltammograms of compounds **DA-1** and **DA-2** ($C_1 = 4 \times 10^{-5}$ M, $C_2 = 4.5 \times 10^{-5}$ M) in CH_2Cl_2 at 100 mV·s^{-1} on a glassy carbon electrode with n-Bu_4NPF_6 (0.1 M).

4. Theoretical calculations

4.1. Geometry optimization

The optimized structures with selected geometry parameters of the most stable *cis* and *trans* isomers for **DA-1** and **DA-2** are presented in Figure 3 (a) and (b), respectively. The relative energies, Gibbs free enthalpies and abundance at room temperature of these minima are collected in Table 1. The PES (Potential Energy Surface) is very flat and the number of local minima is large. It is connected with -OCH$_3$ and -CH$_3$ rotation possibility. We present only the lowest in energy minima for *cis* and *trans* isomers. As one can see the most stable forms of both compounds are *trans-trans* (marked as t-t) isomers and only t-t forms have contribution to population at 298 K. The structures obtained for both compounds are similar and the t-t isomers are almostplanar. The t-c conformers are 21.9 and 22.3 kJ/molhigher in energy for **DA-1** and **DA-2** respectively and they show bended structure. It means that *cis-trans* isomerization is connected with strong structural reorganization in space. The c-t isomers are relatively close in energy to t-c forms (24.1 and 24.3 kJ/mol for **DA-1** and **DA-2** respectively). The *cis-cis* isomers are much higher in energy (64.3 and 64.6 kJ/mol).

Table 1. The calculated relative energies, Gibbs free enthalpies, abundance in 298 K and the $\Delta E^{HOMO-LUMO}$ for **DA-1** and **DA-2** conformers. B3LYP/6-311(d,p).

conformer	ΔE (kJ/mol)	ΔG^{298K} (kJ/mol)	Abundance (%)	$\Delta E^{HOMO\text{-}LUMO}$ (eV)
DA-1 t-t	0.0	0.0	100%	2.078
DA-1 t-c	21.9	23.5	0%	2.091
DA-1 c-t	24.1	26.0	0%	2.159
DA-1 c-c	64.3	65.0	0%	2.163
DA-2 t-t	0.0	0.0	100%	2.019
DA-2 t-c	22.3	26.3	0%	2.027
DA-2 c-t	24.3	28.4	0%	2.070
DA-2 c-c	64.6	65.4	0%	2.068

(a)

DA-1 t-t

DA-1 t-c

DA-1 c-t

DA-1 c-c

(b)

DA-2 t-t

DA-2 t-c

DA-2 c-t

DA-2 c-c
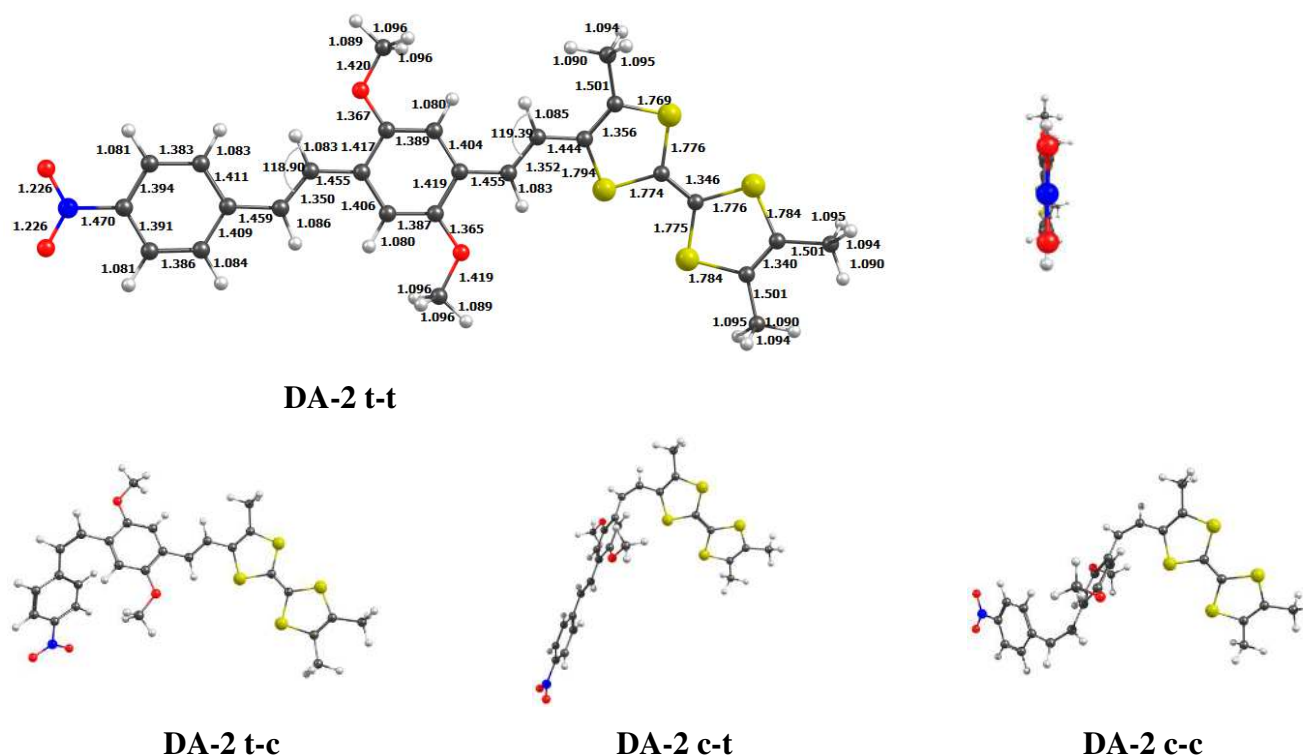
Figure 3. Optimized molecular structures of **DA-1** (a) and **DA-2** (b) conformers with selected geometry parameters. DFT/B3LYP/6-311(d,p). Atom colors labeling: C – dark gray, H – light gray, S - yellow, N – blue, O - red.

4.2. Molecular orbitals

The computed frontier Molecular Orbitals (MO) are rendered in Figure 4. In both compounds the highest occupied molecular orbital (HOMO) is delocalized over electron rich tetrathiafulvalene (TTF) system. In the case of LUMO (lowest unoccupied molecular orbital), one can see that it is delocalized over the π-conjugated spacer and the accepting *p*-nitrophenyl unit with almost no contribution from electron donating TTF group. The HOMO-LUMO energy gap is relatively low and similar for both compounds and it equals 2.08 and 2.02 eV for **DA-1** and **DA-2**, respectively. The $\Delta E^{HOMO-LUMO}$ for the other conformers are given in Table 2. The HOMO → LUMO transition implies an electron density transfer. Moreover, the HOMO-LUMO gap which is relatively low can explain the origin of observed shoulder band in experimental UV-Vis spectra. It indicates that the intramolecular charge transfer (ICT) between the TTF donor and *p*-nitrophenyl acceptor fragment can be responsible for the observed shape of the spectra.

HOMO   **LUMO**

DA-1 t-t
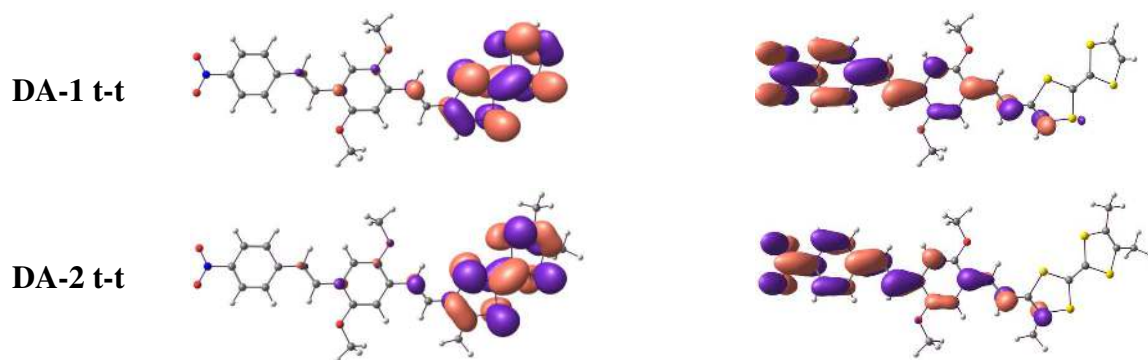
DA-2 t-t

Figure 4. The contour plots (isodensity = 0.02au) of HOMO and LUMO of the **DA-1** and **DA-2** t-t isomers (B3LYP/6-311(d,p) level of theory).

4.3. Computed UV-Visible absorption spectra

The vertical excitations energies were calculated using Time Dependent DFT (TD-DFT) [30] in order to characterize the nature of the electronic transitions and assignment of the observed bands in UV-Visible absorption spectra. Because of some limitations of TD-DTF B3LYP method and high contribution of charge-transfer transitions the calculations have been also carried out by CAM-B3LYP method [31]. Obtained theoretical and experimental results are given in Table 3 and the experimental and simulated spectra are shown in Figure 1.

Table 2. λ_{calc} at B3LYP/6-311(d,p) and CAM-B3LYP/6-311(d,p) (vacuum and DCM solution) and λ_{exp} (thin film and DCM solution) level of theory with assignment of low electronic singlet excitations of **DA-1** and **DA-2 t-t** isomers.

	Absorption wavelength [nm]			Oscillator strength		Transitions (% weight)
	Vacuum		Thin film			
	B3LYP	CAM-B3LYP		B3LYP	CAM-B3LYP	B3LYP
	λ_{calc}	λ_{calc}	λ_{exp}			
DA-1 t-t	676			0.2638		H→L (98%)
	486			0.0124		H-1→L (94%) H→L+1 (2%)
	478	429		1.0728	1.4270	H-1→L (96%) H→L+1 (2%)
	445	386		0.0006	0.0006	H→L+1 (95%) H→L+2 (3%)
	382	372		0.0235	0.3530	H-2→L (69%) H-1→L+1 (25%)
	373	316		0.6642	0.0211	H-3→L (15%) H-2→L (21%)
						H-1 →L+1 (61%)

	DCM/PCM		DCM			B3LYP
	B3LYP	CAM-B3LYP		B3LYP	CAM-B3LYP	
	λ_{calc}	λ_{calc}	λ_{exp}			
	307			0.3054		
	300			0.1140		
DA-2 t-t	697			0.2457		H→L (98%)
	494			0.0200		H→L+1 (94%)
	487	433		1.0781	1.4169	H-1→L (97%)
	450	388		0.0011	0.0019	H→L+2 (95%) H→ L+3 (2%)
	391	373		0.0094	0.3832	H-3→L (4%) H-2→L (79%) H-1→L+1 (13%)
	376	318		0.6137	0.0081	H-3→L (15%) H-2→L (7%) H-1→L+1 (74%)
		308			0.3783	
		297			0.0436	
DA-1 t-t	698			0.3566		H→L (98%)
	522	442		0.9155	1.8300	H-1→L (99%)
	496	380		0.1232	0.0009	H→L+1 (96%)
	438	374		0.0004	0.0823	H→L+2 (92%) H→L+3 (5%)
	402	327		0.1356	0.0257	H-2→L (88%) H-1→L+1 (7%)
	393	312		0.6202	0.4165	H-3→L (8%) H-2→L (6%) H-1→L+1 (83%)
		300			0.0526	
DA-2 t-t	710			0.3420		H→L (99%)
	529	444		0.9361	1.8361	H-1→L (99%)
	498	383		0.1186	0.0018	H+1→L+1 (96%)
	443	372		0.0003	0.0846	H→L+2 (95%) H→L+3 (5%)
	409	327		0.0657	0.0175	H-3→L (4%) H-2→L (88%) H-1→L+1 (5%)
	395	313		0.6547	0.4271	H-3→L (11%) H-2→L (3%) H-1→L+1 (84%)
		297			0.1051	

As it was observed in the case of the Azo-based iminopyridine ligands [32] the calculated wavelengths of low electronic state transitions at CAM-B3LYP level for the dyads **DA-1** and **DA-2** match better to experimental ones relatively to B3LYP. On the other hand the calculated oscillator

strength is reproduced better in B3LYP calculations. In all spectra the most intensive transition corresponds to H-1→L. The CAM-B3LYP simulations lead to underestimation of the higher energy states (H→L). A bathochromic shift in the spectra registered in DCM solution (Figure 1) is observed according to thin film spectra. Note that for the methyl substituted derivative **DA-2** spectrum the H-1→L is also red-shifted.

5. Nonlinear optical properties

5.1. Theoretical nonlinear optical parameters

The nonlinear optical (NLO) properties, such as Second Harmonic Generation (SHG) and Third Harmonic Generation (TGH) are affected by structural features. The properties such as the dipole moment (μ), polarizability (α_{ij}) [equivalent to $\chi^1(0)$] and the first hyperpolarizability (β_{ijj}), [equivalent to $\chi^2(0)$], where ($i, j = x, y, z$) are closely connected to nonlinear optical properties. These parameters were also calculated by DFT/B3LYP method. The obtained values for the most stable conformers and orientation of dipole moments vectors are collected in Table 3. The μ_x, μ_y, μ_z, μ_{total} values and orientation of dipole moments for less stable conformers are collected in Table 1S (Supporting information). We also report the isotropically averaged polarizabilities ($\langle\alpha\rangle$), the polarizability anisotropies ($\Delta\alpha$), and the isotropically first-order hyperpolarizabilities (β_{vec}), which are defined respectively, as [33]:

$$\langle\alpha\rangle = \frac{1}{3}\left(\alpha_{xx} + \alpha_{yy} + \alpha_{zz}\right),$$

$$\Delta\alpha = \left\{\frac{1}{2}\left[\left(\alpha_{xx} - \alpha_{yy}\right)^2 + (\alpha_{xx} - \alpha_{zz})^2 + \left(\alpha_{yy} - \alpha_{zz}\right)^2 + 6\left(\alpha_{xy}^2 + \alpha_{xz}^2 + \alpha_{yz}^2\right)\right]\right\}^{1/2},$$

$$\beta_{vec} = \sqrt{\beta_x^2 + \beta_y^2 + \beta_z^2}, \tag{1}$$

where β_i ($i = x, y, z$) is given by $\beta_i = \left(\frac{1}{3}\right)\sum_{j=x,y,z}\left(\beta_{ijj} + \beta_{jij} + \beta_{jji}\right)$.

Calculated values in the Table 3 show that μ_{tot}, $<\alpha>$, $\Delta\alpha$ for **DA-1** and **DA-2** are similar between themselves which results from the similarity in the structures of these molecules. The first-order hyperpolarizability (β_{vec}) being twice higher in the case of **DA-2** suggests that **DA-2** as compared to **DA-1** can be more efficient in SHG.

Table 3. The calculated dipole moments, polarizabilities and hyperpolarizabilities for **DA-1** and **DA-2 t-t** conformers. The orientation of dipole moment vectors are also shown. B3LYP/6-311(d,p)

DA-1 *t-t*	DA-2 *t-t*

Dipole moment [D]	μ_x	7.07	8.18
	μ_y	0.12	0.27
	μ_z	0.53	1.10
	μ_{tot}	7.09	8.26

Polarizability [Å^3]	α_{xx}	165.1	174.1
	α_{xy}	-7.7	10.0
	α_{yy}	59.1	68.6
	α_{xz}	2.1	2.2
	α_{yz}	-1.0	1.6
	α_{zz}	22.7	27.6
	<α>	82.3	90.1
	$\Delta\alpha$	127.5	129.8

Hyperpolarizability [Å^3]	β_{xxx}	-10400.3	-11636.1
	β_{xxy}	-503.7	-943.1
	β_{xyy}	-19.1	-31.3
	β_{yyy}	6.4	10.4
	β_{xxz}	55.1	147.9
	β_{xyz}	10.8	25.1
	β_{yyz}	2.2	1.0
	β_{xzz}	5.4	15.5
	β_{yzz}	0.9	1.5
	β_{zzz}	2.7	6.6
	β_{vec}[a]	162.5	311.0

[a] β_{vec} is given in 10^{-53} C^3 m^3 J^{-2}

5.2. Nonlinear optical measurements

For the needs of further nonlinear optical measurements (harmonic generation and photoinduced birefringence) samples in the shape of thin polymeric films have been prepared. Typical guest-host system was used, where TTF-based dyads served as an active material. Poly(methyl metacrylate) which exhibits good optical properties, e.g. high transparency, low absorption coefficient in the investigated range and very efficient photostability, was used as the host matrix. Appropriate quantity

of powders (commercially available PMMA and the dyads) was used. At the first stage the **DA-1** and **DA-2** materials were dissolved in DCM solvent and then mixed up in a proper ratio. The final ratio between each dyad and the polymer was 2 % according to the dry mass (w/w). The final solution was used for thin films preparation using a drop casting technique. The resulting mixture was put on a clean silica glass plate and then left in a solvent atmosphere until the end of the solvent evaporation process. Thin films UV-Visible absorption spectra (Figure 5) of the two dyads (**DA-1**/PMMA and **DA-2**/PMMA) have been measured. Also in this figure proper laser modes have been marked where blue (λ = 405 nm) and red (λ = 633 nm) colored lines indicate pumping and reference beams, respectively, which were used in Optical Kerr Effect measurements. Grey (λ = 355 nm) and green (λ = 532 nm) dotted lines indicate generated third and second harmonic of fundamental laser light, respectively. Samples thickness has been measured using profilometer (Tencor, ALFA-Step).
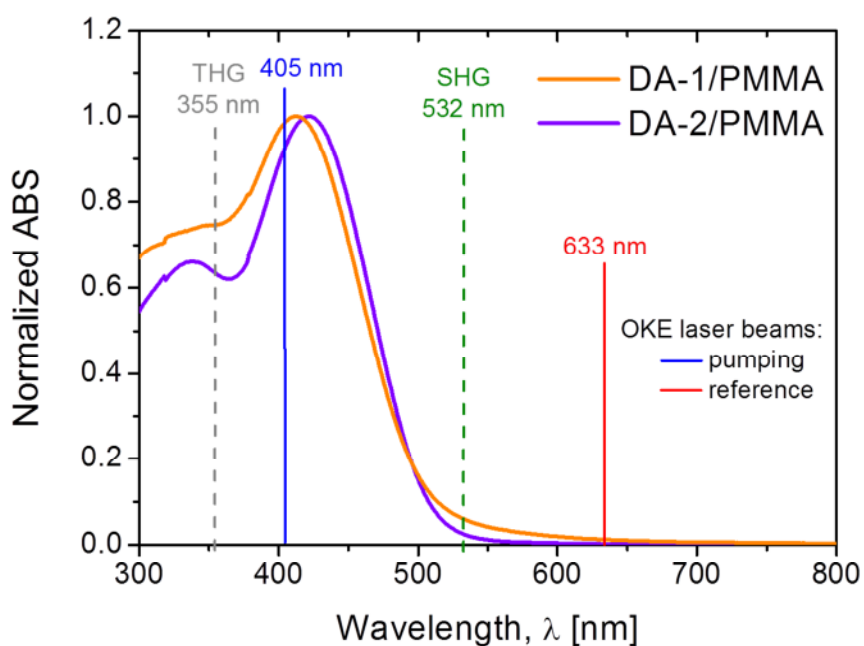

Figure 5. Absorption spectra from thin polymeric films of **DA-1**/PMMA and **DA-2**/PMMA. On the spectra proper laser lines were marked: 405 nm and 633 nm – pumping and reference laser beam from pump-probe OKE experiment; 355 nm and 532 nm – generated harmonics of laser light coming from the samples acquired in THG and SHG experiments.

5.3. Harmonic generation

As the example of the nonlinear optical process, where the energy in the shape of electromagnetic wave can be converted to light generation with doubled and tripled frequency are SHG and THG effects. In general, abovementioned phenomena can be used in various photonic

applications mainly because of the fact that the incident laser beam (incident wavelength) can be converted as follows: $\omega \rightarrow 2\omega$ or $\omega \rightarrow 3\omega$ for SHG and THG, respectively. For the SHG phenomenon the active medium cannot be characterized by inversion symmetry meanwhile for the generation of light with tripled frequency (THG) none symmetry demands are needed to obtain the wave conversion. Such transformations of light have a variety of applications, i.e.: surface nonlinear optics, nonlinear optical microscopy or lasers constructions [34].

Second and third harmonic generation

In figure 7 (a) the typical Maker fringes of SHG in reference material are presented using the *s* polarization mode of incident laser beam. As the reference material for this set of measurements a quartz slab was used. In Figure 6 (b) the SHG signals acquired for the investigated polymeric systems are shown. It is clearly visible that for **DA-1** dyad the frequency doubling process is roughly four times more effective in comparison with the (**DA-2**/PMMA) system. It is also worth to point out that for the *p* polarization mode of the incident beam in both cases the SHG signal is higher.
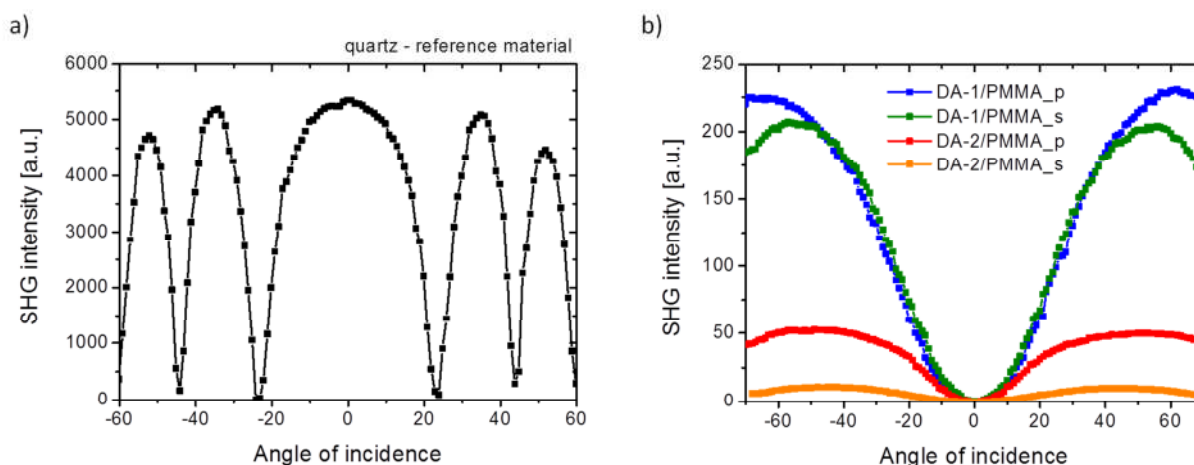

Figure 6. Maker fringes as the characteristic SHG signal coming from the quartz slab – reference material (a) and investigated molecular systems in both polarization modes of incident laser beam – *s* and *p* (b) as the function of rotation angle.

The second step of harmonic generation investigations were the THG measurements. In this case silica glass plate was used as the reference material. Basically, we have used the same experimental set-up with few technical modifications. In this case it was not necessary to pole the films, because THG effect belongs to the 3rd order NLO phenomena, which does not require any symmetrical constraints. As it can be seen in Figure 7 (a), obtained THG Maker fringes of reference material are much more modulated than in the case of SHG measurements due to the less coherence length of

silica in THG process. The two dyads **DA-1** and **DA-2** show THG efficiency about one order of magnitude less than silica (using $\chi^{(3)}$ as the comparable parameter).
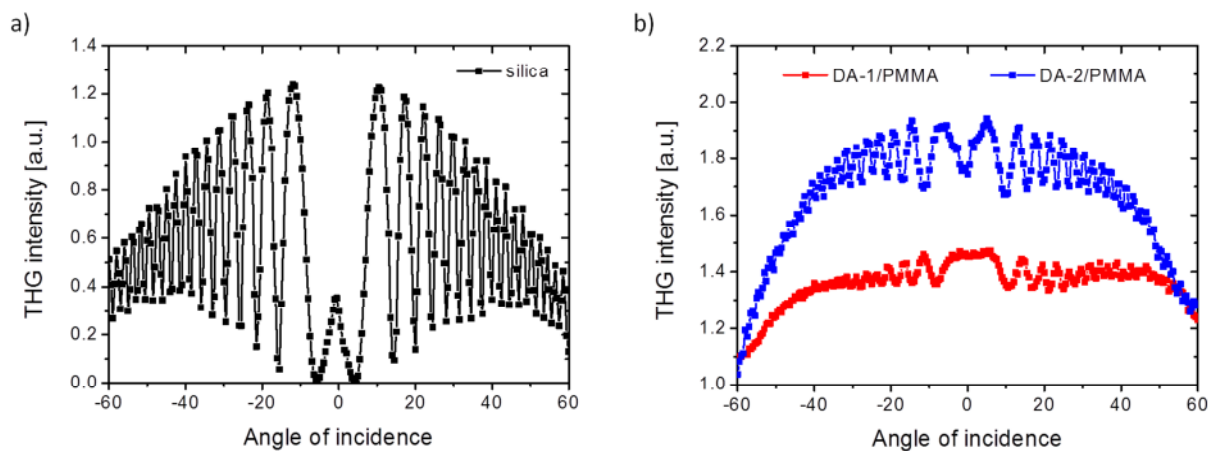

Figure 7. Maker fringes as the characteristic THG signal coming from quartz slab – reference material (a) and investigated molecular systems (b) as the function of rotation angle.

As the result of this step of NLO investigations the second and third order of nonlinear optical susceptibilities have been defined based on the theoretical models of Lee and Kubodera & Kubayashi as described in reference [25], which allowed us to use abovementioned comparable methods for the characterization of our dyads (Table 4) [32]. It seems that differences in chemical structure have a significant impact on the 2nd order NLO response while the opposite situation occurs in the case of THG. It is related to electron cloud distribution, which also has a great impact on molecular alignment realized by corona poling technique before SHG measurements. The positive inductive methyl groups present in **DA-2**/PMMA system affect the charge distribution (also during molecular alignment when high voltage was used), which finally can result in a lower second harmonic response of light generation. Much lighter and less significant than the methyl groups, hydrogen atoms (present in **DA-1**/PMMA system) do not affect so much the charge distribution in the whole structure, especially in the donor region, like in the previous case, which finally also do not change the efficiency of the TTF donating ability. Nevertheless, in this case molecular alignment can be more efficient and give as the result higher SHG signal. With respect to THG investigations the molecular alignment does not play such important role, therefore, it did not affect the final result of $\chi^{(3)}$ parameter and eventually gave very similar results for both investigated compounds (cf. Table 4) - the same order of magnitude for extracted values of 3rd order NLO susceptibilitiy. It is worth to underline that the values of SHG and THG nonlinear optical parameters ($\chi^{(2)}$ and $\chi^{(3)}$) describing the investigated systems are comparable with those of other organic systems (namely: functional polymers or polymers doped organic nonlinear chromophores). The values of the second and/or third

order nonlinear optical susceptibilities are defined on the same or similar order of magnitude in comparison with i.e. azobenzene polymers [35], branched oligothienylenevinylenes derivatives [36], bisdithiafulvenyl-substituted tetrathiafulvalene [37] or polymer (in here: PMMA) doped pyrazoline derivatives [38]. It confirms the potential of the present materials in the field of harmonics of light generation.

Table 4. 2nd and 3rd order nonlinear optical susceptibilities of investigated materials estimated from SHG and THG experiments.

Compound	$\chi^{(2)}$ (s) [a, c] [pm/V]	$\chi^{(2)}$ (p) [a, c] [pm/V]	$\chi^{(3)}$ [b, c] [m^2/V^2]
DA-1	**6.80**	**8.00**	3.75×10^{-23}
DA-2	0.94	2.72	2.04×10^{-23}
silica	---	---	**2.00×10^{-22}**
quartz	**1.00×10^{-12}**	---	---

[a] – calculated according to the used theoretical model, which takes into account the linear absorption coefficient

[b] – calculated according to *Lee* model

[c] – Maker fringes set-up employing the fundamental exit of a 30 ps Nd:YVO$_4$ laser with a repetition rate of 10 Hz at 1064 nm; the energy per pulse was 40 µJ.

5.4. *Optical Kerr Effect*

The results obtained above encouraged us to investigate the Optical Kerr Effect (OKE), which is a third order nonlinear optical effect. This is a typical *pump-probe* experiment, where two different laser lights are used. One of them (pumping one) has to be absorbed by the active material and the other one (the opposite) cannot be absorbed. This later is a reference beam, which transports the information to the photodiode (cf. Figure. 6.). In this experiment it is also possible to define $\chi^{(3)}$ parameter after proper analysis. Optical birefringence is induced inside the material by the second nonlinear refractive index. Therefore, photons which pass through the volume of such material go by two, perpendicular states of polarization and with different velocities, because these two refractive indices are not equal (anisotropy of refractive index is induced). Moreover, the main difference in comparison with SHG is that there are not any structural symmetry demands to cause and observe this effect in the material (like THG and any other 3rd order NLO effects). Among material's characteristics based on the Optical Kerr Effect basically it is possible to distinguish two different

aspects of investigations – dynamics of conformational transformations and photoinduced optical birefringence understood as the photoalignment of molecules in macro scale due to the Malus law (cf. typical OKE experimental set-up with crossed polarizer system) [39] OKE has a lot of various photonic applications, i.e.: all-optical switchers, optical memories and others [40-42]. Results, which describe dynamics of the conformational changes in one of the investigated materials (**DA-2**/PMMA), which were acquired in AC mode on the oscilloscope are presented in Figure 8. As it can be seen in Figure 8 (a) conformational transformations are visible as the uprising and declining signal, which in fact shows transition between low-energy ground state (i.e. *trans* isomer) and high-energy molecular excited state (i.e. *cis* isomer), which is going to relax surplus of energy in various way. It can be typical thermal relaxation leading to obtain the minimum level of energy, which is present in this situation. According to the increasing values of chopper frequency light modulation, the amplitude of measured signal decay is shown in Figure 8 (b). Analogous correlations due to the dynamic conformational changes were done for **DA-1** dyad (see supplementary information - Figure S1).
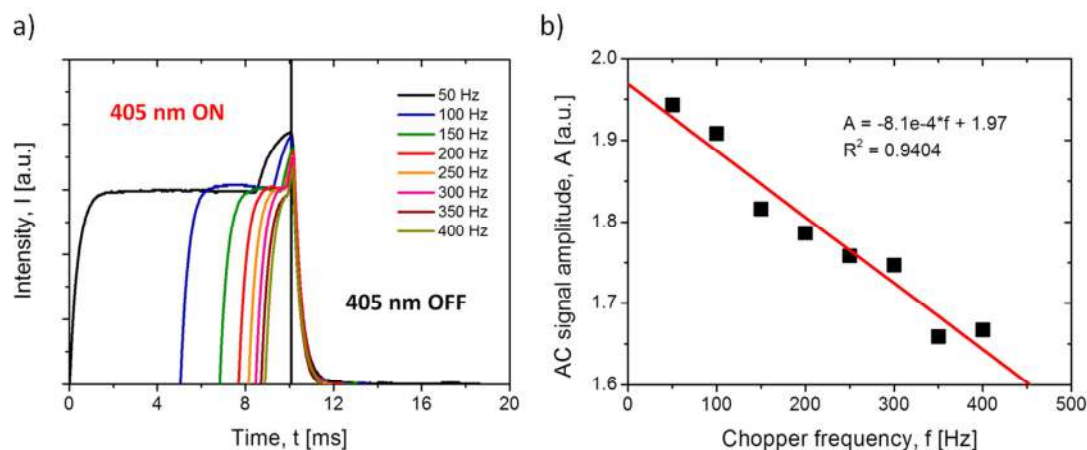

Figure 8. Dynamics of conformational changes (a), OKE AC signal amplitude in frequency function (b) for **DA-2**/PMMA system.

Using the same experimental set-up, but without chopper light modulations we have investigated photoinduced birefringence kinetics in the longer time basis (Figure 9). It allowed us to check the kinetics of the process of creating nonlinear optical refractive index, which causes anisotropy through the material (molecular alignment in the macro scale). After sample illumination by the pumping laser (405 nm ON in Figure 9 (a)) all of the active molecules which are not oriented in a perpendicular direction (long axis of the molecules) due to the polarization state of exciting laser light absorb the portion of photons ($h\nu$). When the free volume is available, molecules are forced to change their molecular direction (due to the same long axis) for perpendicular orientation towards laser light. This behavior is visible on the graph as the signal's uprising. The opposite process

(molecular reorientation according to their thermodynamics), which is achieved by the molecules and which is understood as low as possible energetically state, takes place during thermal relaxation in the dark exposition (signal decay). Based on this, the optical birefringence occurred and transformed reference laser light could go through the crossed polarizer system to the photodiode. Physics of this process (molecular ordering) is the same like with the dynamic changes of conformational states, but the difference that molecules can absorb the pumping laser light and locate themselves for a long time to obtain finally the best possible ordering due to the polarization state of excitation light. As the final effect of pump light illumination, we achieved complete anisotropic system. The uprising pumping beam intensity correlated with the photoinduced birefringence is shown in Figure 9 (b). It is linear function, which means that till the moment of sample degradation process due to the higher excitation intensity it is possible to enhance Δn and obtain more effective and efficient system for all-optical switching. The same set of measurements performed for **DA-1** compound is presented in supplementary information (Figure S2).
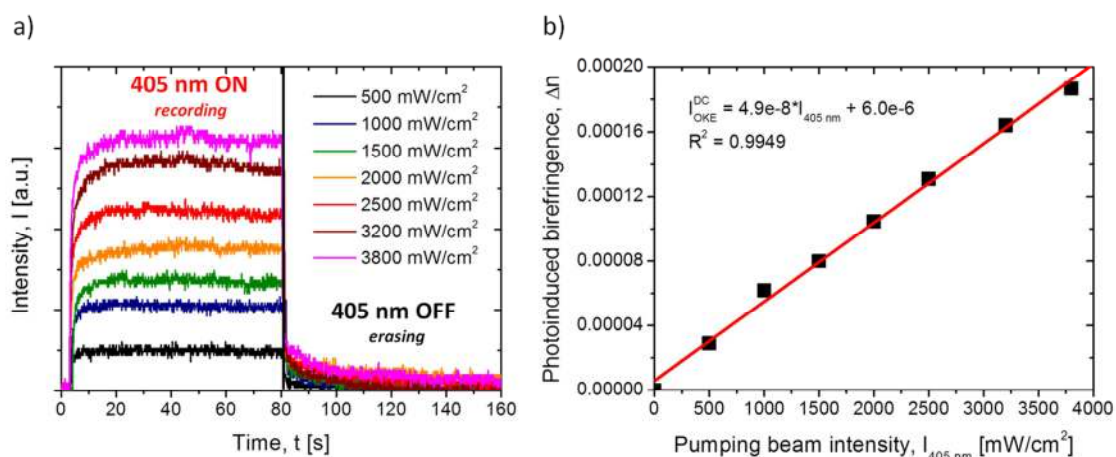

Figure 9. Photoinduced birefringence effect (a) as the function of pumping laser beam intensity (b) for **DA-2**/PMMA system.

In Table 5 we have gathered the most important parameters which were defined based on the Optical Kerr Effect experiments. The 3rd order nonlinear optical susceptibility values and the second refractive index or Kerr constant are of the same order of magnitude for the two investigated dyads. In fact, both molecules exhibit similar chemical structure; therefore it can be assumed that such modifications do not determine different NLO response, which can change significantly physicochemical properties due to the OKE effect. Also the time constants for both dynamic changes of conformational states and photoinduced birefringence are very similar for the two investigated organic systems. It is worth noting that the time constant values (for dynamic mode measurements)

are below half of the millisecond, which indicates that these materials can be used as ultrafast optical switchers, where the response time is a crucial parameter. However, time constant values determined for the long-term molecular ordering are higher than for the previous ones (their values are in the range of seconds regime) and it is typical for the guest-host systems, whereas the matrix branched polymer (in this case PMMA) is used [43]. The experimentally obtained values for the optical birefringence indicate that these kind of D-π-A dyads could be valuable devices components. Moreover, the birefringence can be enhanced after an optimization process, since used excitation intensities did not cause any material's photodegradation changes. The Kerr constant defined for the investigated systems is a typical value for photo-switchable materials in solid states, which is in the order of magnitude equal to $10^{-6} - 10^{-8}$.

Table 5. The 3rd order nonlinear optical susceptibilities and other optical nonlinear parameters of the investigated materials estimated from the pump-probe OKE experiment.

Compound	DA-1	DA-2
$\chi^{(3)}$ [m^2/V^2][a]	4.0×10^{-13}	3.2×10^{-13}
n_2 [m^2/W][a]	5.0×10^{-11}	4.0×10^{-11}
$\chi^{(3)}$ [esu][b]	3.4×10^{-6}	2.9×10^{-6}
n_2 [cm^2/W][b]	6.0×10^{-8}	5.0×10^{-8}
B [m/V^2][c]	5.1×10^{-8}	9.5×10^{-8}
Δn[d]	0.00014	0.00013
t_{grow} [ms] for AC mode	0.34	0.34
t_{decay} [ms] for AC mode	0.35	0.33
t_{grow} [s] for DC mode	3.5	1.4
t_{decay} [s] for DC mode	1.3 [e]	1.3 [e]

[a] – SI unit system; [b] – cgs unit system; [c] – for 2500 mW/cm^2 and 50 Hz modulation; [d] – for 2500 mW/cm^2 ; [e] – low approximation level

6. Conclusions

We have prepared two TTF based D-π-A dyads using multistep synthetic procedure, where the bis-(styryl)benzene system acts as an efficient conjugated π–bridge. The UV-Visible absorption spectroscopy as well as theoretical calculations indicate the occurrence of an intramolecular charge transfer (ICT) between the TTF donor and the nitrophenyl acceptor. According to the gathered

experimental results characterizing nonlinear optical features of the two dyads one main point has to be stressed. The small structural changes, which were present in compounds **DA-1** and **DA-2** basically do not change physiochemical features in a significant meaning. By adding three extra methyl groups mainly in a *donor* part of the dyad **DA-2** it caused very small difference due to the internal electron charge transfer. The effect is not measureable and observable according to the methods which were used for these organic systems. From the same reason the dynamics of photoisomerization process remained very similar for both cases. Small values of the time constants defining abovementioned changes indicate that these groups of materials exhibit a great potential of further exploration in the field of optical switchers construction, where the material's photoresponse time is a crucial parameter.

References

[1] Brédas J-L., Beljonne D., Coropceanu V., Cornil J. Charge-Transfer and Energy-Transfer Processes in π-Conjugated Oligomers and Polymers: A Molecular Picture. Chem Rev 2004;104:4971−5004.

[2] Batail P. Introduction: molecular conductors. Chem Rev 2004;104:4887−90.Special issue on molecular conductors: Chem Rev 2004;104:4887−782.

[3] Martín N. Tetrathiafulvalene: the advent of organic metals. Chem Commun 2013; 49: 7025−27.

[4] Williams J.M., Ferraro J.R., Thorn R.J., Carlson K.D., Geiser U., Wang H.H., Kini A.M., Whangbo M.-H., Organic Superconductors (Including fullerenes), Synthesis, Structure, properties and Theory, Prentice Hall 1992.

[5] Bryce M. R., Murphy L.C., Organic metals Nature 1984;309:119−26.

[6] Canevet D., Sallé M., Zhang G.X., Zhang D.Q., Zhu D.B., Tetrathiafulvalene (TTF) derivatives: key building-blocks for switchable processes. Chem Commun 2009:2245−69.

[7] Nielsen M.B., Lomholt C., Becher J., Tetrathiafulvalenes as building blocks in supramolecular chemistry II. Chem Soc Rev 2000;29:153−64.

[8] Segura J.L., Martin N., New Concepts in Tetrathiafulvalene Chemistry. Angew Chem Int Ed 2001;40:1372−409.

[9] Yamada J., Sugimoto T., TTF Chemistry: Fundamentals & Applications of Tetrathiafulvalene, Kodansha (Tokyo) and Springer (Berlin, Heidelberg, New York), 2004.

[10] Hardouin-Lerouge M., Hudhomme P., Sallé M. Molecular clips and tweezers hosting neutral guests. Chem Soc Rev 2011;40:30−43.

[11] McCall K.L., Morandeira A., Durrant J., Yellowlees L.J., Robertson N., Characterisation of a ruthenium bipyridyl dye showing a long-lived charge-separated state on TiO_2 in the presence of I^-/I_3^-. Dalton Trans 2010;39:4138−45.

[12] Wenger S., Bouit P.-A., Chen Q.L., Teuscher J., Censo D.D., Humphry-Baker R., Moser J.-E., Delgado J.L., Martín N., Zakeeruddin S.M., Grätzel M. Efficient Electron Transfer and Sensitizer Regeneration in Stable π-Extended Tetrathiafulvalene-Sensitized Solar Cells. J Am Chem Soc 2010;132:5164−69.

[13] de Lucas A.I., Martín N., Sánchez L., Seoane C., Andreu R., Garín J., Orduna J., Alcalá R., Villacampa B. The first tetrathiafulvalene derivatives exhibiting second-order NLO properties. Tetrahedron, 1998;54:4655−62.

[14] González M., Segura J.L., Seoane C., Martín N. Tetrathiafulvalene Derivatives as NLO-phores: Synthesis, Electrochemistry, Raman Spectroscopy, Theoretical Calculations, and NLO Properties of Novel TTF-Derived Donor-π-Acceptor Dyads. J Org Chem 2001;66:8872−82.

[15] Fuks-Janczarek I., Luc J., Sahraoui B., Dumur F., Hudhomme P., Berdowski J., Kityk I.V. Third-Order Nonlinear Optical Figure of Merits for Conjugated TTF−Quinone Molecules. J Phys Chem B 2005;109:10179−183.

[16] Sahraoui B., Fuks I., Bartkiewicz S., Matczyszyn K., Mysliwiec J., Kityk I.V., Berdowski J., Allard E., Cousseau J. Enhancement of third-order optical susceptibility of C_{60}-TTF compounds using nematic liquid crystal. Chem Phys Letters 2002;365:327−32.

[17] Sahraoui B, Kityk I.V., Hudhomme P, Gorgues A. Temperature-pressure anomalies of electrooptic coefficients in C-60-TTF derivatives. J Phys Chem B 2001;105:6285−99.

[18] Iliopoulos K., Czaplicki R., El Ouazzani H., Balandier J.Y., Chas M., Goeb S., Sallé M., Gindre D., Sahraoui B. Physical origin of the third order nonlinear optical response of orthogonal pyrrolo-tetrathiafulvalene derivatives. Appl Phys Lett 2010;97:101104−06.

[19] Iliopoulos K, El-Ghayoury A, El Ouazzani H, Pranaitis M, Belhadj E, Ripaud E, Mazari M., Sallé M., Gindre D., Sahraoui B. Nonlinear absorption reversing between an electroactive ligand and its metal complexes. Opt Express 2012;20:25311−6.

[20] Iliopoulos K., Guezguez I., Kerasidou A. P., El-Ghayoury A., Branzea D., Nita G., Avarvari N., Belmabrouk H., Couris S., Sahraoui B. Effect of metal cation complexation on the nonlinear optical response of an electroactive bisiminopyridine ligand. Dyes and Pigments 2014;101: 229–233.

[21] Fabbrini G., Menna E., Maggini M., Canazza A., Marcolongo G., Meneghetti M.. Zinc-Induced Switching of the Nonlinear Optical Properties of a Functionalized Bis(styryl)benzene J Am Chem Soc 2004;126: 6238−39.

[22] Frisch, M. J.; Trucks, G. W.; Schlegel, H. B.; Scuseria, G. E.; Robb, M. A.; Cheeseman, J. R.; Montgomery Jr, J. A.; Vreven, T.; Kudin, K. N.; Burant, J. C.; Millam, J. M.; Iyengar, S. S.; Tomasi, J.; Barone, V.; Mennucci, B.; Cossi, M.; Scalmani, G.; Rega, N.; Petersson, G. A.; Nakatsuji, H.; Hada, M.; Ehara, M.; Toyota, K.; Fukuda, R.; Hasegawa, J.; Ishida, M.; Nakajima, T.; Honda, Y.; Kitao, O.; Nakai, H.; Klene, M.; Li, X.; Knox, J. E.; Hratchian, H. P.; Cross, J. B.; Adamo, C.; Jaramillo, J.; Gomperts, R.; Stratmann, R. E.; Yazyev, O.; Austin, A. J.; Cammi, R.; Pomelli, C.; Ochterski, J. W.; Ayala, P. Y.; Morokuma, K.; Voth, G. A.; Salvador, P.; Dannenberg, J. J.; Zakrzewski, V. G.; Dapprich, S.; Daniels, A. D.; Strain, M. C.; Farkas, O.; Malick, D. K.; Rabuck, A. D.;

Raghavachari, K.; Foresman, J. B.; Ortiz, J. V.; Cui, Q.; Baboul, A. G.; Clifford, S.; Cioslowski, J.; Stefanov, B. B.; Liu, G.; Liashenko, A.; Piskorz, P.; Komaromi, I.; Martin, R. L.; Fox, D. J.; Keith, T.; Al-Laham, M. A.; Peng, C. Y.; Nanayakkara, A.; Challacombe, M.; Gill, P. M. W.; Johnson, B.; Chen, W.; Wong, M. W., Gonzalez, C.; Pople, J. A. Gaussian 09, Revision D.01, Gaussian Inc., Wallingford CT, 2009.

[23] Tomasi J., Mennucci B., Cammi R., Quantum Mechanical Continuum Solvation Models. Chem Rev 2005;105: 2999−3094.

[24] Miertus S., Scrocco E., Tomasi J. Electrostatic interaction of a solute with a continuum. A direct utilizaion of AB initio molecular potentials for the prevision of solvent effects. Chem Phys 1981;55:117−29.

[25] Sahraoui B., Luc J., Meghea A., Czaplicki R., Fillaut J.-L., Migalska-Zalas A. Nonlinear optics and surface relief gratings in alkynyl–ruthenium complexes. J Opt A: Pure Appl Opt 2009;11:024005−26.

[26] Witiak D.T., Loper J.T., Ananthan S., Almerico A.M., Verhoef V.L., Filppi J.A., Mono and bis(bioreductive) alkylating agents: synthesis and antitumor activities in a B16 melanoma model. J Med Chem 1989;32:1636−42.

[27] Garin J., Orduna J., Uriel S., Moore A.J. , Bryce M.R., Wengener S., Yufit D.S., Howard J.A.K. Improved Syntheses of Carboxytetrathiafulvalene, Formyltetrathiafulvalene and (Hydroxymethyl)tetrathiafulvalene:Versatile Building Blocks for New Functionalised Tetrathiafulvalene Derivatives. Synthesis 1993;489−93.

[28] Moore A.J., Bryce M.R., Batsanov A.S., Cole J. C., Howard J.A.K. Functionalised Trimethyltetrathiafulvalene (TriMe-TTF) Derivatives via Reactions of Trimethyltetrathiafulvalenyllithium with Electrophiles: X-ray Crystal Structures of Benzoyl-TriMe-TTF and Benzoylthio-TriMe-TTF. Synthesis 1995;6:675−82.

[29] Park Y.I., Kuo C.-Y., Martinez J.S., Park Y.-S., Postupna O., Zhugayevych A., Kim S., Park J., Tretiak S., Wang H.-L. Tailored Electronic Structure and Optical Properties of Conjugated Systems through Aggregates and Dipole–Dipole Interactions. Appl Mater Interfaces 2013;5: 4685−95.

[30] Scalmani G., Frisch M.J., Mennucci B., Tomasi J., Cammi R., Barone V. Geometries and properties of excited states in the gas phase and in solution: theory and application of a time-dependent density functional theory polarizable continuum model. J Chem Phys 2006;124: 094107:1−15.

[31] Yanai T., Tew D.P., Handy N.C. A new hybrid exchange–correlation functional using the Coulomb-attenuating method (CAM-B3LYP). Chem Phys Chem 2004;393:51−7.

[32] Ayadi A., Branzea D.G., Benmensour M., Boucekkine A., Zouari N., El-Ghayoury A. Azo-based iminopyridine ligands: synthesis, optical properties, theoretical calculations and complexation studies. Tetrahedron 2015;71:7911−19.

[33] Alparone A. Static and Dynamic Electronic (Hyper)polarizabilities of Dimethylnaphthalene Isomers: Characterization of Spatial Contributions by Density Analysis. Scientific World Journal. 2013;2013: 832682

[34] Nonlinear Optics 3rd Edition, Robert W. Boyd. Print Book ISBN: 9780123694706; eBook ISBN: 9780080485966. Publisher: Academic Press ©2008.

[35] El Ouazzani H., Iliopoulos K., Pranaitis M., Krupka O., Smokal V., Kolendo K., Sahraoui B. Second- and Third-Order Nonlinearities of Novel Push-Pull Azobenzene Polymers. J Phys Chem B 2011;115:1944−49.

[36] Fuks-Janczarek I., Nunzi J-M., Sahraoui B., Kityk I.V., Berdowski J., Caminade A.M., Majoral J.-P., Martineau A.C., Frere P., Roncali J. Third-order nonlinear optical properties and two-photon absorption in branched oligothienylenevinylenes. Opt Commun 2002;4-6:461−66.

[37] Sahraoui B., Rivoire G., Terkia-Derdra N., Sallé M., Zaremba J. Third-order nonlinear optical properties of new bisdithiafulvenyl-substituted tetrathiafulvalene. J Opt Soc Am B 1998 ;15:923−28.

[38] Papagiannouli I., Szukalski A., Iliopoulos K., Mysliwiec J., Couris S., Sahraoui B. Pyrazoline derivatives with a tailored third order nonlinear optical response. Rsc Adv 2015;5: 48363−67.

[39] Szukalski A., Haupa K., Miniewicz A., Mysliwiec J. Photoinduced Birefringence in PMMA Polymer Doped with Photoisomerizable Pyrazoline Derivative. J Phys Chem C 2015;119:10007 Scientific World Journal. 2013;2013: 83268−14

[40] Wu S.Z., Lu M., She W.L., Yan K., Huang Z.Z. All-optical switching effect in PVK-based optoelectronic composites. Mater Chem Phys 2004;83:29−33.

[41] Delaire J.A., Nakatani K. Linear and nonlinear properties of photochromic molecules and materials. Chem Rev 2000;100:1817−45.

[42] Okamoto T., Kamiyama T., Yamaguchi I. All-optical spatial light modulator with surface plasmon resonance. Opt Lett 1993;18:1570−72.

[43] Pawlik G., Mitus A.C., Mysliwiec J., Miniewicz A., Grote J.G. Photochromic dye semi-intercalation into DNA-based polymeric matrix: Computer modeling and experiment. Chem Phys Lett 2010;484:321−23.

. **Two TTF based donor-pi-acceptor dyads have been synthesized**

. **Occurrence of an intramolecular charge transfer (ICT) band between the donor and acceptor fragments**

. **High NLO response has been found for the two dyads**

. **The experimental finding have been verified by theoretical calculations**